



HAL
open science

Middle level IM-MS and CIU experiments for improved therapeutic immunoglobulin subclass fingerprinting ACS Paragon Plus Environment Analytical Chemistry

T. Botzanowski, O. Hernandez-Alba, M. Malissard, E. Wagner-Rousset, E. Desligniere, O. Colas, F. Haeuw J., A. Beck, S. Cianferani

► To cite this version:

T. Botzanowski, O. Hernandez-Alba, M. Malissard, E. Wagner-Rousset, E. Desligniere, et al.. Middle level IM-MS and CIU experiments for improved therapeutic immunoglobulin subclass fingerprinting ACS Paragon Plus Environment Analytical Chemistry. Analytical Chemistry, 2020, 92 (13), pp.8827-8835. 10.1021/acs.analchem.0c00293 . hal-02960844

HAL Id: hal-02960844

<https://hal.science/hal-02960844>

Submitted on 8 Oct 2020

HAL is a multi-disciplinary open access archive for the deposit and dissemination of scientific research documents, whether they are published or not. The documents may come from teaching and research institutions in France or abroad, or from public or private research centers.

L'archive ouverte pluridisciplinaire **HAL**, est destinée au dépôt et à la diffusion de documents scientifiques de niveau recherche, publiés ou non, émanant des établissements d'enseignement et de recherche français ou étrangers, des laboratoires publics ou privés.

This document is confidential and is proprietary to the American Chemical Society and its authors. Do not copy or disclose without written permission. If you have received this item in error, notify the sender and delete all copies.

Middle level IM-MS and CIU experiments for improved therapeutic immunoglobulin subclass fingerprinting

Journal:	<i>Analytical Chemistry</i>
Manuscript ID	ac-2020-00293w.R2
Manuscript Type:	Article
Date Submitted by the Author:	n/a
Complete List of Authors:	Botzanowski, Thomas; IPHC Hernandez-Alba, Oscar; IPHC, Laboratoire de Spectrométrie de Masse Bio-Organique (LSMBO) Malissard, Martine; Centre d'Immunologie Pierre Fabre Wagner-Rousset, Elsa; Centre d'Immunologie Pierre Fabre, Physico-Chemistry Deslignière, Evolène; IPHC, Laboratoire de Spectrométrie de Masse Bio-Organique (LSMBO) Colas, Olivier; Centre d'Immunologie Pierre Fabre Haeuw, Jean-François; Centre d'Immunologie Pierre Fabre, Physico-Chemistry Beck, Alain; Centre d'Immunologie Pierre Fabre, Physico-Chemistry Cianférani, Sarah; IPHC, Laboratoire de Spectrométrie de Masse Bio-Organique (LSMBO)

SCHOLARONE™
Manuscripts

Middle level IM-MS and CIU experiments for improved therapeutic immunoglobulin subclass fingerprinting

Thomas Botzanowski^{1¶}, Oscar Hernandez-Alba^{1¶}, Martine Malissard², Elsa Wagner-Rousset², Evolène Deslignière¹, Olivier Colas², Jean-François Haeuw², Alain Beck², Sarah Cianférani^{1*}

¹ Laboratoire de Spectrométrie de Masse BioOrganique, Université de Strasbourg, CNRS, IPHC UMR 7178, 67000 Strasbourg, France.

² IRPF - Centre d'Immunologie Pierre-Fabre (CIPF), 74160 Saint-Julien-en-Genevois, France.

*Corresponding author: Sarah Cianférani. Email: sarah.cianferani@unistra.fr

ABSTRACT: Most of the current FDA and EMA approved therapeutic monoclonal antibodies (mAbs) are based on humanized or human IgG1, 2 or 4 subclasses and engineered variants. On the structural side, these subclasses are characterized by specific inter-chains disulfide bridge connections. Different analytical techniques have been reported to assess intact IgGs subclasses, with recently special interest in native ion mobility (IM) and collision induced unfolding (CIU) mass spectrometry (MS). However, these two techniques exhibit significant limitations to differentiate mAb subclasses at the intact level. In the present work, we aimed at developing a unique IM-MS-based approach for the characterization of mAb subclasses at the middle level. Upon IdeS-digestion, the unfolding patterns of the F(ab')₂ and Fc domains were simultaneously analyzed in a single run to provide deeper structural insights of the mAb scaffold. The unfolding patterns associated with the F(ab')₂ domains are completely different in terms of unfolding energies and number of transitions. Thereby, F(ab')₂ regions are the diagnostic domain to provide specific unfolding signatures to differentiate IgG subclasses and provide more confident subclass categorization than CIU on intact mAbs. In addition, the potential of middle-level CIU was evaluated through the characterization of eculizumab, a hybrid therapeutic IgG2/4 mAb. The unfolding signatures of both domains allowed to corroborate, within a single run, the hybrid nature of eculizumab as well as specific subclass domain assignments to the F(ab')₂ and Fc regions. Altogether, our results confirm the suitability of middle-level CIU of F(ab')₂ domains for subclass categorization of canonical and more complex new generation engineered antibodies and related products.

INTRODUCTION

During the last 20 years, monoclonal antibody (mAb) development and engineering have significantly evolved due to their therapeutic efficiency against many diseases such as cancer, and autoimmune diseases¹. More than 80 antibody-based products are currently approved by regulatory agencies (FDA and EMA), while ~600 others are in clinical studies, including more than 60 in phase III clinical trials².

Among the different post-translational modifications (PTMs) that can occur within the primary sequence of mAbs, glycosylation and inter-chain disulfide linkages strongly contribute to the stabilization of the tertiary structure of these proteins. Indeed, therapeutic mAbs can be classified into four subclasses (IgG1, IgG2, IgG3, and IgG4) with different inter- and intra-chain disulfide connectivities. While human IgG3 subclass is usually not considered for therapeutic mAbs engineering and production due to its limited potential associated to its shorter half-life¹, human IgG1, IgG2, and IgG4 mAb subclasses represent the main classes of mAb-based therapeutics. One of the main structural differences between the three therapeutic subclasses (IgG1, IgG2, and IgG4) is the number (four for IgG1 and IgG4 and six for IgG2) and the connectivities of inter-chain disulfide bridges³ (Figure 1). The heavy and light chains of all subclasses are linked by one

disulfide bond, while the two heavy-chains can be linked either by two (for IgG1 and IgG4) or four (for IgG2) disulfide bonds located in the hinge region of the antibody³. In addition, mAbs global structure is also maintained with 12 intra-chain disulfide bridges that connect two cysteines that belong to the same domain. The inter-chain disulfide bridges network, which is characteristic of each individual subclass, has an impact on different mAb properties (structure, stability, surface hydrophobicity, isoelectric point, etc.)⁴ and modulate their higher-order structure⁵⁻⁸. Thereby, mAbs from different subclasses will differ in their secondary immune functions⁹⁻¹⁰. In terms of mAb developability, there is a continuous interest for improvement of new analytical techniques to characterize the impact of the different inter-chain disulfide patterns on therapeutic mAb structures and structure-function relationships.

Ion mobility coupled to mass spectrometry (IM-MS), and its collision induced unfolding (CIU) variant, have been used to characterize the structure and dynamics of proteins¹¹⁻¹⁴ and protein complexes¹⁵⁻¹⁶ in the gas-phase. During the last 5 years, CIU has been increasingly used in structural biology to characterize a wide range of biological systems and has integrated the analytical portfolio of international regulatory agencies¹⁷. Although the CIU approach still remains as a laborious and time-consuming process, significant efforts have

been made to improve data acquisition¹⁸ and interpretation¹⁹⁻²⁰. CIU experiments allowed to circumvent in some cases the limitations associated to IM resolution to separate and differentiate mAbs with very similar global structure. Thereby, CIU afforded structural insights that led to the differentiation of human non-therapeutic mAb subclasses^{20, 22}, ADCs' characterization²³⁻²⁴, and stabilized vs wild-type therapeutic IgG4 mAbs among others²⁵. More particularly, the group of Ruotolo reported that glycan moieties contribute to the stabilization of the mAb scaffold in the gas-phase, thus glycosylated mAbs require around 15% more energy to undergo unfolding compared to their non-glycosylated counterparts²². The same study also highlighted the role of inter-chain disulfide linkage in mAb gas-phase stability, the latter being proposed as responsible of differences observed on CIU patterns from four human mAb subclasses²². However, in some cases, the CIU-based categorization/characterization of intact mAb subclasses remains challenging due to the very subtle differences observed in their intact CIU fingerprints.

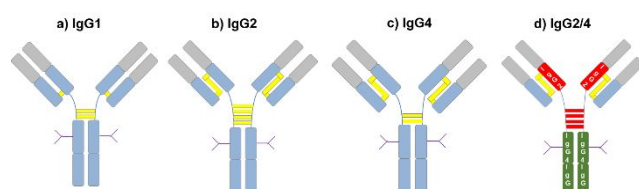


Figure 1 : Schematic representation of inter-chain disulfide bridges (yellow bars) characteristic of the IgG1 (a), IgG2 (b), IgG4 (c) and hybrid IgG2/4 (d) mAb subclasses.

In the present work, we aimed at improving IM-MS and CIU workflows to better differentiate the subclasses of therapeutic mAbs (IgG1, IgG2, and IgG4), including engineered hybrid mAbs. For this purpose, we developed middle-level IM-MS and CIU approaches where the mAb scaffold is IdeS-digested²⁶ prior to IM-MS or CIU analysis. In this case, a thorough characterization of therapeutic mAbs scaffold is performed based on the individual analysis of the F(ab')₂ and Fc subdomains. The global structure along with the gas-phase dynamics associated with each subunit highlighted the structural similarities/differences induced by the inter-chain connectivities of each therapeutic subclass, and provided more evidences to improve mAb subclass differentiation. Finally, the middle-level CIU allowed to unravel the subclass of a hybrid engineered mAb, pinpointing its suitability to characterize and differentiate the subclass of canonical and hybrid therapeutic mAbs.

MATERIALS AND METHODS

Sample preparation

Eculizumab (Soliris, Alexion Pharmaceuticals Inc.), panitumumab (Vectibix, Amgen) natalizumab (Tysabri, Biogen), adalimumab (Humira, Abbvie), trastuzumab (Herceptin, Roche), ipilimumab (Yervoy, BMS), and reslizumab (Cinqair, Teva Pharmaceuticals) were sourced from their respective manufacturers as EMA-approved drug products. N-glycans were enzymatically removed to obtain more homogeneous native mass spectra. Thereby mAbs were

N-deglycosylated during 30 min at 37 °C with IgZERO (Genovis). In the case of middle-level analysis, the deglycosylated mAbs were degraded with IdeS enzyme (immunoglobulin-degrading enzyme of *Streptococcus pyogenes*, FabRICATOR, Genovis). A 1 µg/unit ratio was used to achieve an efficient digestion and subsequently, the mixture was incubated during 60 min at 37°C. After deglycosylation and/or IdeS digestion, therapeutic mAbs were then desalted against 100 mM ammonium acetate at pH 7.0 prior to native MS analysis, using about six to eight cycles of centrifugal concentrator (Vivaspin, 30 kDa cutoff, Sartorius, Göttingen, Germany). The concentration of each individual solution after desalting process was measured by UV absorbance using a nanodrop spectrophotometer (Thermo Fisher Scientific, France). Prior to native MS analysis, each sample was diluted in 100 mM ammonium acetate at pH 7.0 to a final concentration of 5 µM.

Native MS analysis

Native mass spectra were acquired on an Orbitrap Exactive Plus EMR (Thermo Fisher Scientific, Bremen, Germany) coupled to an automated chip-based nanoelectrospray device (Triversa Nanomate, Advion, Ithaca, USA) operating in the positive ion mode. The capillary voltage and the pressure of the nebulizer gas were set at 1.7-1.9 kV and 0.15-0.20 psi, respectively. The source parameters were tuned in order to obtain best mass accuracy for native MS experiments as followed: briefly, the in-source voltage was set to 150 eV, the HCD cell voltage was fixed to 50 eV and the pressure of the backing region was fixed to 2 mbar. Native MS data interpretations were performed using Xcalibur™ software v4.0 (Thermo Fisher Scientific, Bremen, Germany).

Native IM-MS and CIU experiments

Ion mobility and CIU experiments were performed on a hybrid Q-IM-TOF mass spectrometer (Synapt G2, Waters, Manchester, UK). The cone voltage was fixed at 80 V to improve the ion transmission and avoid in source ion activation. The backing pressure of the Z-spray source was set to 6 mbar and the argon flow rate was 5 mL/min. Ions were cooled and separated in the IM cell with a Helium flow rate of 120 mL/min and a N₂ flow rate of 60 mL/min. Ion mobility parameters were tuned to improve ion separation and prevent ion heating as described in *Hernandez et al*²⁵. Briefly, the wave velocity and height were fixed to 800 m/s and 40 V, respectively. IM drift times of each mAb were converted in collision cross sections using three charge states of concanavalin A, pyruvate kinase and alcohol dehydrogenase as external calibrants as reported elsewhere²⁷. The drift times of the reference proteins and the analytes ions were measured under the same experimental conditions. MassLynx software (Waters, Manchester, U.K.) was used to generate arrival time distributions.

Collision induced unfolding experiments were performed by increasing the collision voltage of the trap by 5 V steps from 0 to 200 V prior to IM separation. All data were acquired consecutively on the same subclass mAb batch with strictly identical instrumental parameters to reduce fluctuations in the backing, trap and IM pressures. Individual IM data were gathered to generate CIU fingerprint using the last version of CIUSuite2 software (version 2.1) and in particular the CIUSuite2_BasicAnalysis and the CIUSuite2_StabilityAnalysis modules in order to obtain

average and differential plots, and then to determine CIU50 values to assess the stability of each transition directly from the CIU data. Each plot corresponds to the average of the three analysis replicates with a root mean square deviation lower than 10 % showing a good reproducibility of the experiment. ATD intensities were normalized to a maximum value of 1 and classical smoothing parameters were used (Savitzky-Golay algorithm with a window length of 3 and a polynomial order of 2) as used in the previous version of the software. Prior to subclass classification and CIU comparison, the centroid of the ATDs at zero volts were standardized (same initial IM centroid) to provide a straightforward comparison of the unfolding patterns. Adalimumab, panitumumab, and natalizumab were chosen as the IgG1, IgG2, and IgG4 reference mAbs, respectively to create the in-house classification methods at both, intact, and middle levels using the CIUSuite2 algorithm. Four additional therapeutic mAbs (eculizumab, trastuzumab, ipilimumab, and reslizumab), from different mAb subclasses, were included in the present study to evaluate the reliability of our in-house classification methods. Three CIU replicates of all mAbs were used to generate the whole dataset. Collision voltages with the highest score in the univariate feature selection plot (UFS) were specifically selected^{19, 28} to provide an adequate classification of clusterized mAbs (eculizumab, trastuzumab, ipilimumab, and reslizumab).

RPLC analysis

Separation of the different IgG1, IgG2, IgG2/4 and IgG4 subclasses were performed in a Zorbax RRHD column (2.1 mm x 50 mm, 1.8 μm , 300 \AA) from Agilent Technologies (Wilmington, DE, USA). The column was loaded with 1 μL of the intact mAbs solution at 5 mg/ml final concentration (5 μg). Mobile phase A was composed of 0.1% TFA, 2% isopropyl alcohol (IPA) in water, and mobile phase B was 0.1% TFA, 25% acetonitrile, in IPA. Samples were eluted with a constant flow rate of 250 $\mu\text{L}/\text{min}$ and using a chromatographic gradient from 10 to 25% B over 9 minutes, followed by a shallow gradient up to 27.8% B over 7 min. Then, the gradient increased up to 29.8% B over 1 minute, followed by 29.8 – 50% B over 2 minutes.

nrCE-SDS analysis

IgGs were analyzed in non-reduced condition using a MauriceTM system (Protein Simple) equipped with the CompassTM software. Chemicals were provided from the MauriceTM CE-SDS application kit from the provider. Samples were diluted in 1x sample buffer to a final concentration of 1 mg/mL, from which 50- μL -aliquot samples were made. Then 2 μL of internal standard was added to each sample. 2.5 μL of a 250-mM stock solution of the alkylating agent IAM was added to each 50- μL sample to block disulfide scrambling or exchange. They were denatured at 70 $^{\circ}\text{C}$ for 10 minutes, cooled on ice for 5 minutes and mixed by vortex. Each sample was then transferred to a 96-well plate and spun down in a centrifuge for 10 minutes at 1000 x g. All samples were electrokinetically injected into the cartridge capillary by applying 4600 V for 20 seconds before separation by electrophoresis at 5750 V during 35 min. Electropherograms were analyzed with the EmpowerTM data software.

Differential scanning calorimetry (DSC)

DSC experiments were performed on a MicroCal VP-Capillary DSC instrument (Malvern Instruments). Samples were buffer exchanged into PBS Dulbecco pH 7.4 buffer or 25 mM His/His-HCl, 150 mM NaCl, pH 6.5 and diluted to 1 mg/mL in according buffer. 400 μL of the protein solution as well as 400 μL of the according buffer were dispensed in 96 well plates, loaded to the capillary sample cell while the reference cell contained the corresponding buffer. The chamber was pressurized to 3 atm and the temperature ramped from 40 $^{\circ}\text{C}$ to 100 $^{\circ}\text{C}$ at 1 $^{\circ}\text{C}/\text{min}$ heating rate. The recorded DSC thermograms were baseline subtracted and subjected to a multi-component Gaussian fitting in the MicroCal VP-Capillary DSC software 2.0 (Malvern Instruments).

The temperatures for three major transitions were extracted from the fitted Gaussian models, relating to the unfolding of CH2, Fab, and CH3 domains. For each sample, 3 independent experiments were carried out allowing us to use a value of 1 $^{\circ}\text{C}$ as the cutoff limit for evaluating the significance of the differences observed in melt temperatures.

RESULTS AND DISCUSSION

Intact level IM-MS and CIU experiments for mAb subclass classification.

Since mAb glycosylation induces additional heterogeneity on mass spectra without affecting subclass determination by intact-CIU fingerprints²², we first analyzed three deglycosylated mAbs - adalimumab (IgG1), panitumumab (IgG2), and natalizumab (IgG4) – at the intact level by native MS (Figure S1) and IM-MS (Figure S2). Overall, the charge state distributions observed on the native mass spectra are centered either on the 24+ or 23+ charge states. The same therapeutic mAbs were next analyzed by native IM-MS at the intact level to provide more insights into their global conformation. For all charge states, IM-MS provides very similar $^{\text{TW}}\text{CCS}_{\text{N}_2}$ values within the error of the CCS measurement, avoiding classification of subclasses on the sole basis of CCS measurements. The co-elution of all reference therapeutic mAbs upon IM separation leads to the conclusion that current TWIMS resolution cannot afford an efficient differentiation of the three subclasses as previously reported on non-therapeutic mAbs^{22, 25} (Figure S2a). Of note, even though the centroid of the collision cross section distribution (CCSD) profiles are very similar, the FWHM of the IgG2 CCSD is slightly broader (1.65 nm^2 versus 1.10 nm^2 , and 1.15 nm^2 for IgG1 and IgG4, respectively), suggesting potential co-existence of several isomers, in agreement with a more flexible IgG2 scaffold. The high similarity in terms of primary sequence between these mAbs leads to the analysis of quasi-isobaric (< 2 % mass difference) and quasi-iso-cross sectional (< 1 % CCS difference) (Figure S2b, c) proteins for which classical native IM-MS instrumentation can only provide limited information.

As differences in CIU fingerprints of different mAb subclasses from human serum were mainly related to differences in the number and connectivities of inter-chain disulfide bridges contained within the structure of mAbs^{20, 22}, we next performed and compared CIU experiments on the three therapeutic mAbs at the intact level (Figure 2). Overall the CIU patterns of the three mAb subclasses look very similar with two unfolding transitions present on the three CIU fingerprints.

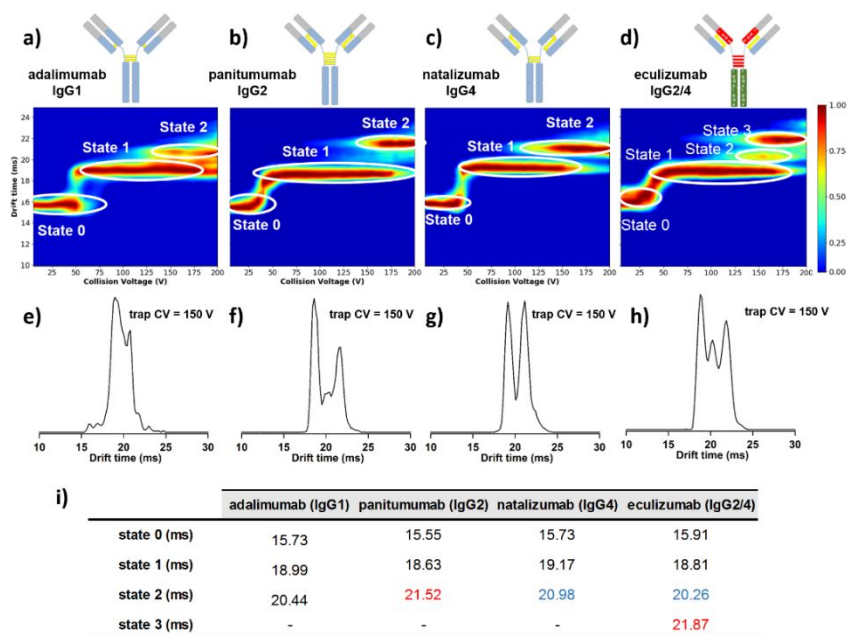


Figure 2: Intact level CIU experiments. CIU experiments of the 22+ charge state of adalimumab (IgG1) (a), panitumumab (IgG2) (b), natalizumab (IgG4) (c), and hybrid IgG2/4 eculizumab (d). CIU fingerprints are depicted in the upper panels. ATDs extracted at 150 V corresponding to the three therapeutic mAbs are depicted in the lower panels (e, f, g, and h). Table summarizing the IM drift times of the observed unfolding states (i).

While the three canonical mAb subclasses (adalimumab, panitumumab, and natalizumab) exhibit the same IM migration times at the ground state, some subtle differences can be observed upon ion activation (Figure 2a-c). One diagnostic CIU region is comprised between 100-200 V range where ATDs from the three subclasses exhibit different distributions (Figure 2e-g), allowing the discrimination of the therapeutic mAb subclasses at the intact level, as previously reported^{20, 22, 25}. Although mAb subclasses can be differentiated when these structures populate excited unfolding states upon activation with the background gas, CIU fingerprints at the intact level only provide very limited and subtle differences, hindering a clear-cut classification of therapeutic mAb subclasses.

Middle-level CIU analysis affords easier mAb subclass categorization than intact CIU.

In order to circumvent intact level IM-MS and CIU limitations, we next performed native IM-MS and CIU experiments (Figure 3, 4, and 5) at the middle level to further characterize the global conformation and the gas-phase stability of the $F(ab')_2$ and Fc domains of IdeS-digested adalimumab, panitumumab, and natalizumab (see Material and Method section).

Regarding IM-MS results, the measured $^{TW}CCS_{N_2}$ of the $F(ab')_2$ domains (20+ and 21+ charge states) are very similar (average differences in CCS comprised between 0.66 and 2.62%), which avoids clear assessment of mAb subclass based solely on $^{TW}CCS_{N_2}$ measurements. While broad CCSD exhibiting two distributions were observed for the $F(ab')_2$ domain of IgG1 and IgG4 mAbs (the second feature being most likely due to gas phase activation), only one narrow CCS distribution is observed for the IgG2 panitumumab (Figure 3).

For the 12+ charge state of the Fc region, the measured $^{TW}CCS_{N_2}$ are $33.1 \pm 0.1 \text{ nm}^2$, $33.2 \pm 0.1 \text{ nm}^2$ and $33.1 \pm 0.1 \text{ nm}^2$ for IgG1, IgG2 and IgG4 references respectively (Figure S3), showing that the categorization/characterization of IgG1, IgG2, and IgG4 mAb subclasses cannot be performed based on the $^{TW}CCS_{N_2}$ measurements of the Fc domains. These results ($^{TW}CCS_{N_2}$ measurements along with CCSDs) prompted us to suggest that the only potential information that might be deduced directly from IM-MS data is that IgG2 subclass might be differentiated from IgG4/IgG1 with the $F(ab')_2$ regions.

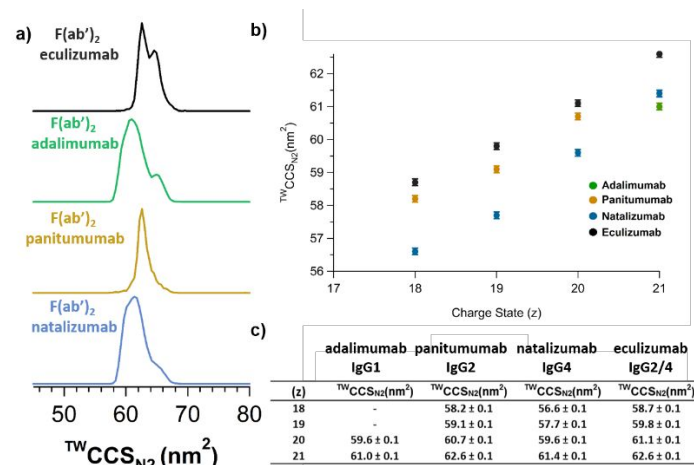


Figure 3: Middle-level IM-MS analysis of $F(ab')_2$ domains. CCSDs of the 21+ charge state of the $F(ab')_2$ domains of eculizumab, adalimumab, panitumumab, and natalizumab (a). Evolution of the $F(ab')_2$ $^{TW}CCS_{N_2}$ as a function

of the charge state (b). Table summarizing the measured $^{TW}CCS_{N_2}$ of the $F(ab')_2$ domains (c).

We next compared CIU experiments on both $F(ab')_2$ and Fc subunits of adalimumab, panitumumab, and natalizumab after IdeS digestion (Figure 4 and Figure 5, respectively). Overall, the differentiation of the mAb subclasses upon collisional activation of the $F(ab')_2$ domains is clearly evidenced based not only on the number of unfolding transitions observed in the CIU fingerprints, but also due to the different collision energies associated with each transition (Figure 4). While only two unfolding transitions are observed in the CIU fingerprint of the IgG2 $F(ab')_2$ domain (17.9 V and 37.6 V, respectively) (Figure 4b), three transitions are observed in the case of the IgG1 $F(ab')_2$ domain (23.6 V, 67.3 V, and 123.5 V respectively)

CIU fingerprints than on intact CIU plots, leading to more reliable classification.

For the Fc domains, CIU fingerprints of the three reference mAbs (adalimumab, panitumumab, and natalizumab) exhibit very similar unfolding patterns with two unfolding transitions that lead to an increase of the collision cross section, and a final transition around 120 V where the global conformation of the Fc domain is compacted (Figure 5). Therefore, relatively low UFS scores were obtained for Fc domain-based subclass categorization (Figure S4c), revealing that clusterization of therapeutic mAbs based on CIU fingerprints of Fc domains might lead to inaccurate subclass differentiation. This result is

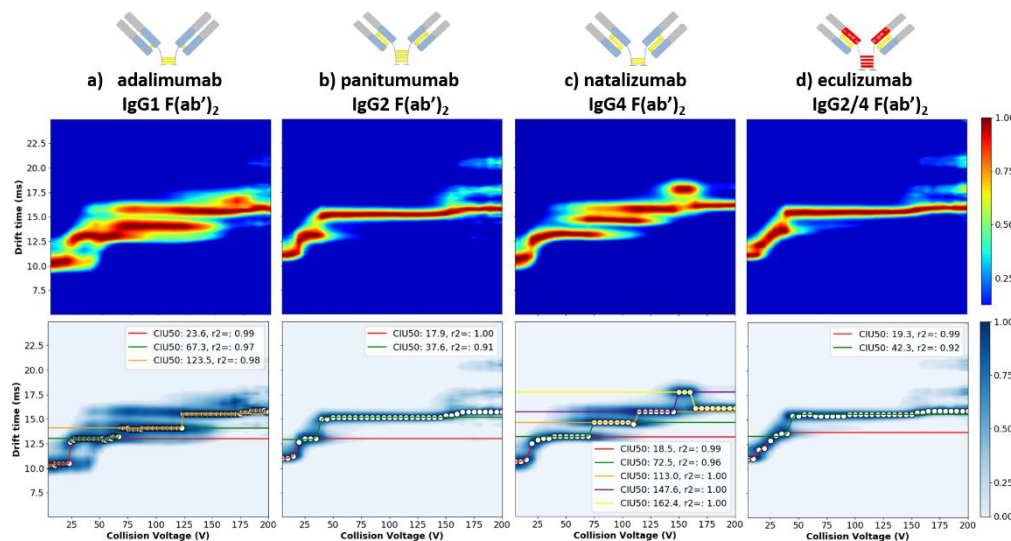


Figure 4: Middle-level CIU experiments on $F(ab')_2$ domains. CIU fingerprints (top panel) and stability analysis “CIU50” of 21+ charge state of $F(ab')_2$ domain of IgG1 (a), IgG2 (b), IgG4 (c), and IgG2/4 (d) from 0 to 200 V trap collision voltage. Gaussian fitting and collision voltages associated with the unfolding transitions are depicted in the lower panels

(Figure 4a), and five transitions in the IgG4 $F(ab')_2$ CIU fingerprint (18.5 V, 72.5 V, 113.0 V, 147.6 V, and 162.4 V) (Figure 4c). The most unfolded state of the IgG2 $F(ab')_2$ domain is populated at lower voltages compared to the IgG1, and IgG4 subclasses. However, this final state is kinetically stabilized from 40 to 200 V, whereas the different unfolded states of IgG1, and IgG4 subclasses are only kinetically stabilized during shorter voltage ranges. The gas-phase stability of the $F(ab')_2$ domain of the IgG2 subclass stems more likely from the higher number of disulfide bridges in the hinge region (four inter-chain S-S) that prevents the unfolding process of the domain upon ion heating. Our data thus suggest that middle-level CIU patterns of $F(ab')_2$ domains allow easier and more confident subclass determination than intact level CIU fingerprints. This is also supported by the UFS plots obtained from CIUSuite2 comparing the classification methods for intact mAbs and the $F(ab')_2$ subunits (Figure S4). While all the UFS scores of the intact-CIU method are lower than 1.5, suggesting relatively similar subclasses, the $F(ab')_2$ UFS plot shows a highly diagnostic region between 60 and 140 V with higher scores (-log p-values > 1.5), pinpointing higher differences in $F(ab')_2$

consistent with the high similarity (~95%) of the Fc sequence between the three subclasses (Table S1) leading to very similar gas-phase stabilities and dynamics. However, the collision energy associated to the unfolding transitions observed on the IgG1 Fc fingerprint (41.5 V, 86.4 V, and 131.5 V) are slightly higher compared to those observed in the IgG2 (25.0 V, 67.5 V, and 122.5 V) and IgG4 (27.7 V, 67.5 V, 117.4 V) Fc domains suggesting a slightly higher gas-phase stabilization of the IgG1 Fc domain. This observation might be related to the influence of the non-covalent interactions that contribute to the stabilization and dimerization of the mAb Fc domain²⁹⁻³³. Indeed, the strongest CH3-CH3 interaction was found in the IgG1 structure (up to 10^6 -fold) in comparison to the other subclasses²⁹, which is in good agreement with the gas-phase stability observed in the Fc CIU fingerprints. To strengthen this hypothesis, stability of the constant regions was also investigated using differential scanning calorimetry (DSC) (Table S2)²³. In this case, the melting temperatures corresponding to the denaturation of the CH2 and CH3 domains of the different mAbs subclasses evidenced a higher thermal stability for the IgG1 heavy chain constant domains, in

agreement with results obtained by middle-level CIU experiments.

Altogether, our middle level CIU results on three model mAbs depict that middle level CIU patterns of $F(ab')_2$ domains generated after IdeS digestion enable more easy and confident subclass classification than intact level CIU data.

indicated to treat the rare hemolytic disease paroxysmal nocturnal hemoglobinuria³⁴. The heavy-chain constant region of the parental antibody was repaved with components of both human IgG2 and IgG4 constant regions. The heavy chain of the hybrid mAb includes the CH1 and hinge regions of human IgG2 fused to the CH2 and CH3 regions of human IgG4. To avoid the

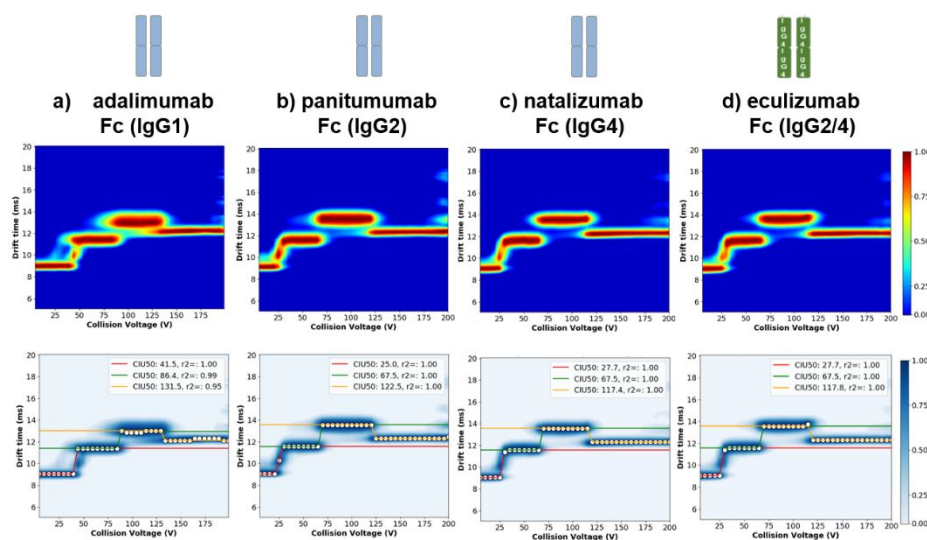


Figure 5: Middle-level CIU experiments on Fc domains. CIU fingerprint of 12+ charge state of Fc domains corresponding to adalimumab (IgG1) (a), panitumumab (IgG2) (b), natalizumab (IgG4) (c), and eculizumab (IgG2/4) (d). The CIU fingerprints and the corresponding Gaussian fitting are depicted in upper and lower panels respectively.

Validation/Benchmarking of middle-level $F(ab')_2$ CIU pattern for better mAb subclass assessment.

To strengthen our claims, we performed additional middle level CIU experiments on $F(ab')_2$ domains of three additional therapeutic mAbs: two IgG1 (trastuzumab and ipilimumab) and one IgG4 (reslizumab), no additional IgG2 being available for inclusion in this validation phase. This series of different therapeutic mAbs was subjected to our in-house mAb classification method based on the three reference mAbs previously detailed (adalimumab, panitumumab and natalizumab) (Figure S5). After selection of the most diagnostic collision voltages of the $F(ab')_2$ reference fingerprints (from 60 to 140 V), our middle-level CIU classification method led to the unambiguous identification of trastuzumab and ipilimumab as IgG1 (with $77.0 \pm 14.2\%$ and $90.8 \pm 8.7\%$, respectively) and reslizumab as IgG4 ($97.1 \pm 0.2\%$ of confidence) (Figure S5 g-i). Even though the CIU fingerprints of the different mAbs from the same subclass do not exhibit strictly the same unfolding features, most likely due to the contribution of the specific variable domains of the $F(ab')_2$ regions²⁵ of each mAb, middle-level CIU of $F(ab')_2$ domains afforded clear-cut subclass identification and categorization of therapeutic mAbs.

Middle level CIU strategies provide accurate characterization of eculizumab, a hybrid IgG2/4

Finally, to challenge our middle-level CIU method based on $F(ab')_2$ sub-classification, we analyzed eculizumab, as a model for hybrid mAb constructs. Eculizumab is a humanized hybrid IgG2/4 mAb directed against the complement protein C52 and

generation of an antigenic site during the fusion, a restriction endonuclease cleavage site common to both IgG2 and IgG4 was used to join the two constant regions (31 amino acids flanking the fusion site are identical between IgG2 and IgG4)³⁵. The unique combination of an IgG2/4 constant region makes this molecule fail to bind to Fc receptors (IgG2) and does not activate complement cascade (IgG4), which reduces the pro-inflammatory potential of the antibody³⁶. Due to its inherent hybrid constitution, classical analytical techniques used for intact-mAb subclass categorization applied to eculizumab characterization provide a series of unclear/contradictory results. For example, non-reduced capillary electrophoresis-sodium dodecyl sulfate (nrCE-SDS) eculizumab analysis presents a single peak which is rather in agreement with an IgG4 than with an IgG2 nrCE-SDS behavior for which doublet peaks are expected (Figure S6)³⁷. Conversely, reversed-phase high performance liquid chromatography (rpHPLC) analysis of eculizumab clearly presents an IgG2-like behavior with three peaks reflecting IgG2 structural isoforms A, B and A/B (Figure S7)³⁸⁻³⁹. As classical analytical methods for intact mAb characterization are not adapted to depict and dissect the complex structural scaffold of hybrid mAb formats, there is a need for complimentary analytical techniques able to tackle this issue. We thus applied our CIU workflows for eculizumab characterization.

Regarding the ^{13}C CCS_{N2} measurements and as expected from our results on reference IgGs, hybrid eculizumab cannot be differentiated from reference therapeutic mAbs at the intact-

level owing to their similar global conformations (overall difference in CCS < 2%, Figure S2). Interestingly, a broad CCSD (FWHM=1.42 nm²) is observed for eculizumab. In addition a small shoulder is also depicted on the right side of its CCSD, which might be related to the presence of different ion populations. At the middle-level, independently of the charge state, the ^{TW}CCS_{N₂} of the F(ab')₂ region of eculizumab is closer to those of the IgG2 reference (panitumumab), which might be considered as a first hint towards eculizumab F(ab')₂ region behaving as an IgG2 (Figure 3b, and c). As expected, no conclusions can be drawn from middle level native IM-MS ^{TW}CCS_{N₂} measurements regarding the Fc part of eculizumab owing to the high primary sequence similarity (~95%) with the three mAbs (Table S1, and Figure S3). Altogether IM-MS investigation provides very limited information towards the characterization of the “hybridicity” of eculizumab.

We thus moved to CIU experiments. Intact-level CIU fingerprint of eculizumab (hybrid IgG2/IgG4) was compared to those of adalimumab, panitumumab and natalizumab (references IgG1, IgG2, and IgG4, respectively) previously described (Figure 2d). Overall, eculizumab CIU fingerprint shows four unfolding states and three transitions, revealing one additional unfolding transition compared to the reference IgG2 or IgG4 subclasses. In more details, the first transition occurs at 36.6 V, the second at ~145 V and the last one at 168 V. Automated subclass classification using the CIUSuite2 module⁴⁰ mainly recognizes eculizumab as an IgG2 (Figure S8d). However, the classification algorithm is not well adapted to characterize the hybrid structure of eculizumab since there is not a significant correlation between eculizumab's fingerprint and a secondary mAb subclass (either IgG1, or IgG4). Indeed, the IgG1, and IgG2 subclasses equally contribute to the unfolding pattern of the hybrid mAb (8.5 ± 2.7 and 11.8 ± 3.0 %), which impedes to assess the second most prevailing mAb subclass in eculizumab structure. Interestingly, a closer manual data interpretation allowed highlighting that the first CIU transition of eculizumab (37 V) is similar to the first transition of IgG2 or IgG4, while the two other eculizumab transitions correspond to the second transition of reference IgG4 (145 V for eculizumab versus 147 V) or IgG2 (168 V), respectively, which might suggest that eculizumab CIU fingerprint could result from a composite/hybrid of the two IgG4 and IgG2 CIU patterns. This first evidence can be strengthened based on the centroid IM drift times of each unfolding state. The IM drift time of the second state of eculizumab is similar to the drift time of the second state of natalizumab (blue values in Figure 2i) while the drift time of the third state of eculizumab is close to the second unfolding state drift time of panitumumab (red values in Figure 2i). These data suggest that eculizumab gas-phase unfolding behaviour is hybrid between reference IgG2 and IgG4 mAbs. However, even if intact level CIU allows concluding that eculizumab CIU fingerprint is clearly different from reference IgG2/IgG4 ones, it does not allow to draw any conclusion about the origin of this difference related to its inherent “hybridicity”.

We finally performed CIU experiments on the F(ab')₂ and Fc subunits of eculizumab obtained upon IdeS digestion (Figure 4, and Figure 5). Overall, the CIU fingerprint of the F(ab')₂ subdomain of eculizumab exhibits a very similar CIU pattern (same number of unfolding transitions at very similar collision energies) with the reference IgG2 F(ab')₂ (Figure 4b and d),

suggesting an IgG2-like gas-phase unfolding of eculizumab F(ab')₂. Automatic subclass classification algorithm included in the open source CIUSuite2 software¹⁹ (Figure S8h) assessed the F(ab')₂ subdomain of eculizumab F(ab')₂ as an IgG2-type CIU pattern (79.3 ± 11.3 % of IgG2). These results corroborate middle-IM-MS CCS measurements, and clearly show that the (Fab')₂ of eculizumab can be unambiguously associated to an IgG2 subclass.

For the Fc subdomains, as expected, very similar CIU patterns were observed for all mAbs (Figure 5). Automatic subclass detection of the CIUSuite2 software¹⁹ revealed that eculizumab Fc unfolding pattern was slightly closer to the Fc subdomain of the IgG4 reference (natalizumab) rather than the IgG1 or IgG2 ones (Figure 5, and S8). These subtle but significant differences stem on the very close collision energies associated with each individual unfolding transitions observed in the eculizumab and IgG4 Fc fingerprints (27.7 V, 67.5 V and 117.8 V for eculizumab compared to 27.7 V, 67.5 V and 117.4 V for the reference IgG4). Conversely, all voltages associated to IgG1 unfolding pattern were significantly higher when compared to eculizumab, while only one voltage associated to the third unfolding event allows distinguishing eculizumab (117.8 V) from IgG2 (122.5 V) (Figure 5, and S8). Thereby, the resulting RMSD upon comparison of the eculizumab Fc CIU fingerprint with the three references, IgG1, IgG2, and IgG4, were 28.08 %, 8.84 %, and 4.50 %, respectively, suggesting that the unfolding behavior of the Fc part of eculizumab resembles to an IgG4-like subclass. These results were also corroborated after using the classification algorithm. Upon selection of the most significant collision voltages (45 V, and 135 V), the Fc fingerprint of eculizumab is recognized as an IgG4 at (84,2 ± 2.8 %).

Altogether, our results clearly demonstrate that middle-level CIU probed the duality/hybridicity of engineered mAbs formats. In our case, among all tested analytical techniques (nrCE-SDS, rpHPLC-UV, native IM-MS and CIU-IM-MS at the intact level), middle-level CIU experiments was able to provide structural evidences of eculizumab hybrid format and to assess the subclass of each of its domains, all in one single run. The energy associated with the unfolding transitions along with the number of unfolding events present on F(ab')₂ and Fc CIU fingerprints afforded an accurate and straightforward identification of eculizumab hybrid construction.

CONCLUSIONS

This work presents an alternative and complimentary IM-MS-based approach for mAb subclass distinction. Indeed, as all mAb subclasses have signature peptides, subclass confirmation usually consists of peptide mass fingerprinting after enzymatic digestion⁴¹⁻⁴². To investigate mAb subclass on intact entities, a panel of classical analytical techniques like capillary electrophoresis and liquid chromatography are available. However, ambiguous or even controversial results can be obtained, especially when new formats like hybrid mAbs are concerned. As mAb subclass identification can also be addressed by IM-MS based approaches^{20, 43}, this study presents a middle-level (after IdeS digestion of mAbs) IM-MS strategy based on CIU experiments to tackle mAb subclassification. We demonstrate here that middle-level CIU affords better

distinction of mAb subclasses than similar analyses performed at the intact level.

Considering IM-MS and CCS measurements at both intact and middle levels, mAb subclasses usually present “co-drifting”/overlapping ATDs when using commercially available IM-MS instruments due to a lack of IM resolution, which prevents subclass classification through a simple CCS measurement. Slight differences in ATD profiles and/or ATDs FWHM might eventually suggest rough trends.

In this study, we demonstrate how the analysis of large mAb fragments (50-100 kDa) can be used to compliment native protein CIU datasets. Indeed, stronger conclusions for mAb subclass determination were obtained from middle-level CIU experiments, especially from $F(ab')_2$ CIU pattern interpretation (100 kDa). As the vibrational energy redistribution is more efficient upon collision of the smaller $F(ab')_2$ and Fc domains with the background gas, the ions in the gas-phase can populate additional excited unfolding states, which provide clear-cut specific signature characteristics of mAb subclasses. Conversely to CIU fingerprints of therapeutic mAbs recorded at the intact level that only present subtle differences in the 100-200 V region, $F(ab')_2$ CIU fingerprints exhibit significantly different unfolding features both in terms of number and associated energies of unfolding transitions along the whole voltage range (from 0 to 200 V). As a consequence, the $F(ab')_2$ CIU fingerprints can be considered as the most diagnostic region to differentiate mAb subclasses since the number of unfolding transitions and their associated energies are clearly different for IgG1, IgG2 and IgG4 mAbs. The unfolding behavior of the $F(ab')_2$ domains is mainly related to subclass specific inter-chain disulfide connectivities that drive specific structures, leading to diagnostic CIU features. The influence of the variable domains in the CIU patterns of the $F(ab')_2$ subunits is also observed when comparing CIU fingerprints from the same mAb subclass (IgG1 or IgG4), however, similar unfolding features among each mAb subclass are detected, allowing their classification.

Although CIU unfolding patterns of Fc domains (50 kDa) are overall very similar owing to the absence of covalent connectivities in Fc domains (no inter-chain S-S bridges that connect Fc noncovalent dimers) and the high primary sequence similarities of Fc regions (> 93% in our study), minor differences can also be detected between middle-level CIU fingerprints of Fc domains. Indeed, a careful and detailed data interpretation of transition energies related to non-covalent dimeric Fc domains also affords distinguishing: i) IgG1 from IgG2 or IgG4, with overall higher unfolding energies for all transition states for IgG1 and ii) IgG2 from IgG4 on the basis of one unique transition (the more energetic at 117.4 V for IgG4 versus 122.5 V for IgG2). Ranking of gas-phase stabilities and resistance to unfolding of Fc non-covalent dimers (IgG1>IgG2>IgG4) were directly correlated to strength of noncovalent CH₃-CH₃ interactions. Our results thus show that middle CIU fingerprints are not only sensitive to covalent connectivities (disulfide bridges) differences that drive mAb structure and rigidity ($F(ab')_2$ domains) but also to non-covalent interactions (Fc domains).

Benefits of middle IM-MS and CIU approaches are illustrated for the characterization of hybrid mAb-formats like the IgG2/IgG4 eculizumab. While classical analytical

techniques used for intact mAb subclass validation such as nrCE-SDS or rpHPLC-MS led to controversial results and failed in identifying the hybridicity of eculizumab, intact-level CIU approach provided a first strong hint towards a composite IgG2/IgG4 CIU pattern. The precise hybrid IgG2/IgG4 character of eculizumab was definitely, more clearly and accurately assessed by middle-level CIU. Analysis of the middle-level CIU fingerprints of eculizumab pointed out that the $F(ab')_2$ unfolding pattern corresponds to an IgG2-like mAb reference, confirming the trends identified in middle IM-MS analysis, while the Fc domain behaves as an IgG4-like subclass. For eculizumab, middle-level CIU experiments allowed to face the challenge of hybrid mAb-format characterization, allowing within one single CIU experiment to identify specific structural subclass features but also to attribute subclass to its corresponding mAb subdomain.

Altogether, our results highlight the suitability of middle-level CIU experiments to differentiate and classify the subclass of large mAb fragments, including complex new generation hybrid formats. Middle-level CIU provides more informative insights that enables a further characterization of therapeutic proteins to overcome the limitation of classical analytical techniques used for intact or large mAb fragments. We believe that the analysis of large mAb fragments by middle-level CIU provides unique information content that can not only assist in the analysis of new mAb hybrids but beneficially expand the current IM-MS and CIU method toolbox.

ASSOCIATED CONTENT

Supporting Information

Supporting information Table S1, Table S2, Figure S1, Figure S2, Figure S3, Figure S4, Figure S5, Figure S6, Figure S7 and Figure S8 are available free of charge.

AUTHOR INFORMATION

Corresponding Author

*Phone: +33 (0)3 68 85 26 79. Fax: +33 (0)3 68 85 27 81.

*E-mail: sarah.cianferani@unistra.fr

Author Contributions

*(T.B., O.H.A.) These authors contributed equally.

Notes

The authors declare no competing financial interest.

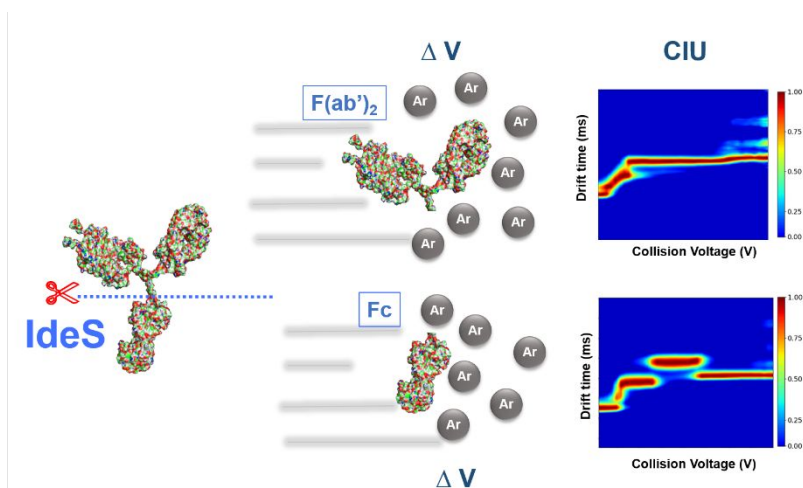
ACKNOWLEDGMENT

This work was also supported by the CNRS, the University of Strasbourg, the “Agence Nationale de la Recherche” (ANR-13-BSV8-0017-01), the French Ministry for Education and Research, and the French Proteomic Infrastructure (ProFI; ANR-10-INBS-08-03). The authors would like to thank GIS IBiSA and Région Alsace for financial support in purchasing a Synapt G2 HDMS instrument. T.B. and O.A.-H. acknowledge the Institut de Recherches Internationales Servier and the IDeX program of the University of Strasbourg for funding of their PhD and postdoctoral fellowship, respectively.

REFERENCES

1. Beck, A.; Goetsch, L.; Dumontet, C.; Corvaia, N., Strategies and challenges for the next generation of antibody drug conjugates. *Nature Reviews Drug Discovery* **2017**, *16* (5), 315-337.
2. Kaplon, H.; Muralidharan, M.; Schneider, Z.; Reichert, J. M., Antibodies to watch in 2020. *Mabs* **2020**, *12* (1).
3. Jefferis, R., Antibody therapeutics: isotype and glycoform selection. *Expert Opin. Biol. Ther.* **2007**, *7* (9), 1401-1413.
4. Liu, H. C.; May, K., Disulfide bond structures of IgG molecules Structural variations, chemical modifications and possible impacts to stability and biological function. *Mabs* **2012**, *4* (1), 17-23.
5. Saphire, E. O.; Parren, P.; Pantophlet, R.; Zwick, M. B.; Morris, G. M.; Rudd, P. M.; Dwek, R. A.; Stanfield, R. L.; Burton, D. R.; Wilson, I. A., Crystal structure of a neutralizing human IgG against HIV-1: A template for vaccine design. *Science* **2001**, *293* (5532), 1155-1159.
6. Ryazantsev, S.; Tischenko, V.; Nguyen, C.; Abramov, V.; Zav'yalov, V., Three-Dimensional Structure of the Human Myeloma IgG2. *Plos One* **2013**, *8* (6).
7. Scapin, G.; Yang, X. Y.; Prorise, W. W.; McCoy, M.; Reichert, P.; Johnston, J. M.; Kashi, R. S.; Strickland, C., Structure of full-length human anti-PD1 therapeutic IgG4 antibody pembrolizumab. *Nature Structural & Molecular Biology* **2015**, *22* (12), 953-958.
8. Zhang, A. M.; Fang, J.; Chou, R. Y. T.; Bondarenko, P. V.; Zhang, Z. Q., Conformational Difference in Human IgG2 Disulfide Isoforms Revealed by Hydrogen/Deuterium Exchange Mass Spectrometry. *Biochemistry* **2015**, *54* (10), 1956-1962.
9. Beck, A.; Wurch, T.; Bailly, C.; Corvaia, N., Strategies and challenges for the next generation of therapeutic antibodies. *Nature Reviews Immunology* **2010**, *10* (5), 345-352.
10. Vafa, O.; Gilliland, G. L.; Brezski, R. J.; Strake, B.; Wilkinson, T.; Lacy, E. R.; Scallon, B.; Teplyakov, A.; Malia, T. J.; Strohl, W. R., An engineered Fc variant of an IgG eliminates all immune effector functions via structural perturbations. *Methods* **2014**, *65* (1), 114-126.
11. Pierson, N. A.; Clemmer, D. E., An IMS-IMS threshold method for semi-quantitative determination of activation barriers: Interconversion of proline cis <-> trans forms in triply protonated bradykinin. *Int. J. Mass spectrom.* **2015**, *377*, 646-654.
12. Shelimov, K. B.; Jarrold, M. F., Conformations, unfolding, and refolding of apomyoglobin in vacuum: An activation barrier for gas-phase protein folding. *J. Am. Chem. Soc.* **1997**, *119* (13), 2987-2994.
13. Shelimov, K. B.; Clemmer, D. E.; Hudgins, R. R.; Jarrold, M. F., Protein Structure in Vacuo: Gas-Phase Conformations of BPTI and Cytochrome c. *J. Am. Chem. Soc.* **1997**, *119* (9), 2240-2248.
14. Clemmer, D. E.; Hudgins, R. R.; Jarrold, M. F., NAKED PROTEIN CONFORMATIONS - CYTOCHROME-C IN THE GAS-PHASE. *J. Am. Chem. Soc.* **1995**, *117* (40), 10141-10142.
15. Ben-Nissan, G.; Vimer, S.; Tarnavsky, M.; Sharon, M., Chapter Nine - Structural mass spectrometry approaches to study the 20S proteasome. In *Methods Enzymol.*, Hochstrasser, M., Ed. Academic Press: 2019; Vol. 619, pp 179-223.
16. Hall, Z.; Politis, A.; Bush, M. F.; Smith, L. J.; Robinson, C. V., Charge-State Dependent Compaction and Dissociation of Protein Complexes: Insights from Ion Mobility and Molecular Dynamics. *J. Am. Chem. Soc.* **2012**, *134* (7), 3429-3438.
17. Kerr, R. A.; Keire, D. A.; Ye, H., The impact of standard accelerated stability conditions on antibody higher order structure as assessed by mass spectrometry. *mAbs* **2019**, *11* (5), 930-941.
18. Migas, L. G.; France, A. P.; Bellina, B.; Barrann, P. E., &ITORIGAMI&IT: A software suite for activated ion mobility mass spectrometry (aIM-MS) applied to multimeric protein assemblies. *Int. J. Mass spectrom.* **2018**, *427*, 20-28.
19. Polasky, D. A.; Dixit, S. M.; Fantin, S. M.; Ruotolo, B. T., CIUSuite 2: Next-Generation Software for the Analysis of Gas-Phase Protein Unfolding Data. *Anal. Chem.* **2019**, *91* (4), 3147-3155.
20. Vallejo, D. D.; Polasky, D. A.; Kurulugama, R. T.; Eschweiler, J. D.; Fjeldsted, J. C.; Ruotolo, B. T., A Modified Drift Tube Ion Mobility-Mass Spectrometer for Charge-Multiplexed Collision-Induced Unfolding. *Anal. Chem.* **2019**, *91* (13), 8137-8146.
21. Atmanene, C.; Petiot-Becard, S.; Zeyer, D.; Van Dorsselaer, A.; Hannah, V. V.; Sanglier-Cianferani, S., Exploring Key Parameters to Detect Subtle Ligand-Induced Protein Conformational Changes Using Traveling Wave Ion Mobility Mass Spectrometry. *Anal. Chem.* **2012**, *84* (11), 4703-4710.
22. Tian, Y. W.; Han, L. J.; Buckner, A. C.; Ruotolo, B. T., Collision Induced Unfolding of Intact Antibodies: Rapid Characterization of Disulfide Bonding Patterns, Glycosylation, and Structures. *Anal. Chem.* **2015**, *87* (22), 11509-11515.
23. Tian, Y. W.; Lippens, J. L.; Netirojjanakul, C.; Campuzano, I. D. G.; Ruotolo, B. T., Quantitative collision-induced unfolding differentiates model antibody-drug conjugates. *Protein Sci.* **2019**, *28* (3), 598-608.
24. Botzanowski, T.; Erb, S.; Hernandez-Alba, O.; Ekhkirch, A.; Colas, O.; Wagner-Rousset, E.; Rabuka, D.; Beck, A.; Drake, P. M.; Cianferani, S., Insights from native mass spectrometry approaches for top- and middle- level characterization of site-specific antibody-drug conjugates. *mAbs* **2017**, *9* (5), 801-811.
25. Hernandez-Alba, O.; Wagner-Rousset, E.; Beck, A.; Cianferani, S., Native Mass Spectrometry, Ion Mobility, and Collision-Induced Unfolding for Conformational Characterization of IgG4 Monoclonal Antibodies. *Anal. Chem.* **2018**, *90* (15), 8865-8872.
26. Chevreux, G.; Tilly, N.; Bihoreau, N., Fast analysis of recombinant monoclonal antibodies using IdeS proteolytic digestion and electrospray mass spectrometry. *Anal. Biochem.* **2011**, *415* (2), 212-214.
27. Bush, M. F.; Hall, Z.; Giles, K.; Hoyes, J.; Robinson, C. V.; Ruotolo, B. T., Collision Cross Sections of Proteins and Their Complexes: A Calibration Framework and Database for Gas-Phase Structural Biology. *Anal. Chem.* **2010**, *82* (22), 9557-9565.
28. Polasky, D. A.; Dixit, S. M.; Vallejo, D. D.; Kulju, K. D.; Ruotolo, B. T., An Algorithm for Building Multi-State Classifiers Based on Collision Induced Unfolding Data. *Anal. Chem.* **2019**, *91* (16), 10407-10412.

29. Rispens, T.; Davies, A. M.; Ooijevaar-de Heer, P.; Absalah, S.; Bende, O.; Sutton, B. J.; Vidarsson, G.; Aalberse, R. C., Dynamics of Inter-heavy Chain Interactions in Human Immunoglobulin G (IgG) Subclasses Studied by Kinetic Fab Arm Exchange. *J. Biol. Chem.* **2014**, *289* (9), 6098-6109.
30. Labrijn, A. F.; Rispens, T.; Meesters, J.; Rose, R. J.; den Bleker, T. H.; Loverix, S.; van den Bremer, E. T. J.; Neijssen, J.; Vink, T.; Lasters, I.; Aalberse, R. C.; Heck, A. J. R.; van de Winkel, J. G. J.; Schuurman, J.; Parren, P., Species-Specific Determinants in the IgG CH3 Domain Enable Fab-Arm Exchange by Affecting the Noncovalent CH3-CH3 Interaction Strength. *J. Immunol.* **2011**, *187* (6), 3238-3246.
31. Rispens, T.; Ooijevaar-de Heer, P.; Bende, O.; Aalberse, R. C., Mechanism of Immunoglobulin G4 Fab-arm Exchange. *J. Am. Chem. Soc.* **2011**, *133* (26), 10302-10311.
32. Wilkinson, I. C.; Fowler, S. B.; Machiesky, L.; Miller, K.; Hayes, D. B.; Adib, M.; Her, C.; Borrok, M. J.; Tsui, P.; Burrell, M.; Corkill, D. J.; Witt, S.; Lowe, D. C.; Webster, C. I., Monovalent IgG4 molecules Immunoglobulin Fc mutations that result in a monomeric structure. *Mabs* **2013**, *5* (3), 406-417.
33. Rose, R. J.; Labrijn, A. F.; van den Bremer, E. T. J.; Loverix, S.; Lasters, I.; van Berkel, P. H. C.; van de Winkel, J. G. J.; Schuurman, J.; Parren, P.; Heck, A. J. R., Quantitative Analysis of the Interaction Strength and Dynamics of Human IgG4 Half Molecules by Native Mass Spectrometry. *Structure* **2011**, *19* (9), 1274-1282.
34. Rother, R. P.; Rollins, S. A.; Mojcik, C. F.; Brodsky, R. A.; Bell, L., Discovery and development of the complement inhibitor eculizumab for the treatment of paroxysmal nocturnal hemoglobinuria (vol 25, pg 1256, 2007). *Nat. Biotechnol.* **2007**, *25* (12), 1488-1488.
35. An, Z. Q.; Forrest, G.; Moore, R.; Cukan, M.; Haytko, P.; Huang, L. Y.; Vitelli, S.; Zhao, J. Z.; Lu, P.; Hua, J.; Gibson, C. R.; Harvey, B. R.; Montgomery, D.; Zaller, D.; Wang, F. B.; Strohl, W., IgG2m4, an engineered antibody isotype with reduced Fc function. *Mabs* **2009**, *1* (6), 572-579.
36. Wong, E. K. S.; Kavanagh, D., Anticomplement C5 therapy with eculizumab for the treatment of paroxysmal nocturnal hemoglobinuria and atypical hemolytic uremic syndrome. *Translational Research* **2015**, *165* (2), 306-320.
37. Guo, A.; Han, M.; Martinez, T.; Ketchem, R. R.; Novick, S.; Jochheim, C.; Balland, A., Electrophoretic evidence for the presence of structural isoforms specific for the IgG2 isotype. *Electrophoresis* **2008**, *29* (12), 2550-2556.
38. Dillon, T. M.; Ricci, M. S.; Vezina, C.; Flynn, G. C.; Liu, Y. D.; Rehder, D. S.; Plant, M.; Henkle, B.; Li, Y.; Deechongkit, S.; Varnum, B.; Wypych, J.; Balland, A.; Bondarenko, P. V., Structural and functional characterization of disulfide isoforms of the human IgG2 subclass. *J. Biol. Chem.* **2008**, *283* (23), 16206-16215.
39. Resemann, A.; Liu-Shin, L.; Tremintin, G.; Malhotra, A.; Fung, A.; Wang, F.; Ratnaswamy, G.; Suckau, D., Rapid, automated characterization of disulfide bond scrambling and IgG2 isoform determination. *Mabs* **2018**, *10* (8), 1200-1213.
40. Polasky, D. A.; Dixit, S. M.; Fantin, S. M.; Ruotolo, B. T., CIUSuite 2: Next-Generation Software for the Analysis of Gas-phase Protein Unfolding Data. *Anal Chem* **2019**.
41. Li, H.; Ortiz, R.; Tran, L.; Hall, M.; Spahr, C.; Walker, K.; Laudemann, J.; Miller, S.; Salimi-Moosavi, H.; Lee, J. W., General LC-MS/MS Method Approach to Quantify Therapeutic Monoclonal Antibodies Using a Common Whole Antibody Internal Standard with Application to Preclinical Studies. *Anal. Chem.* **2012**, *84* (3), 1267-1273.
42. Furlong, M. T.; Ouyang, Z.; Wu, S.; Tamura, J.; Olah, T.; Tymiak, A.; Jemal, M., A universal surrogate peptide to enable LC-MS/MS bioanalysis of a diversity of human monoclonal antibody and human Fc-fusion protein drug candidates in pre-clinical animal studies. *Biomed. Chromatogr.* **2012**, *26* (8), 1024-1032.
43. Niu, S.; Ruotolo, B. T., Collisional unfolding of multiprotein complexes reveals cooperative stabilization upon ligand binding. *Protein Sci.* **2015**, *24* (8), 1272-1281.



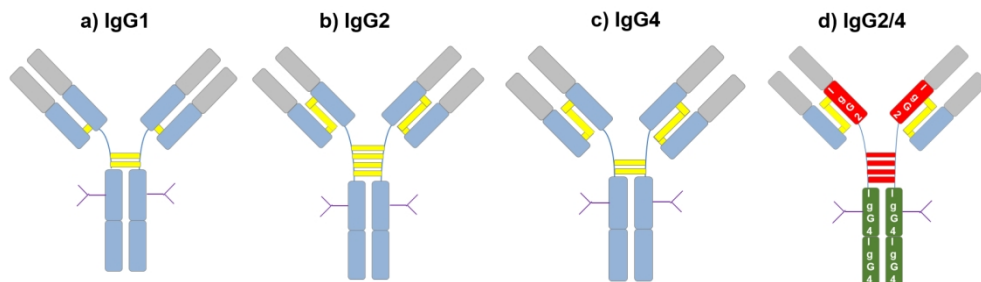


Figure 1 : Schematic representation of inter-chain disulfide bridges (yellow bars) characteristic of the IgG1 (a), IgG2 (b), IgG4 (c) and hybrid IgG2/4 (d) mAb subclasses.

309x94mm (150 x 150 DPI)

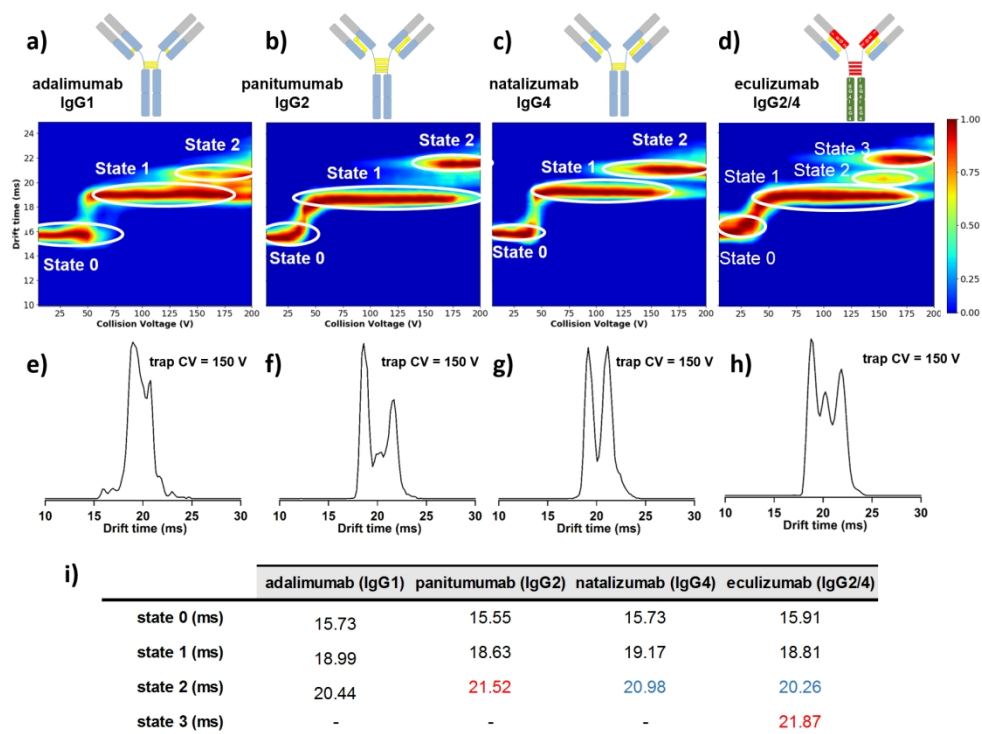


Figure 2: Intact level CIU experiments. CIU experiments of the 22+ charge state of adalimumab (IgG1) (a), panitumumab (IgG2) (b), natalizumab (IgG4) (c), and hybrid IgG2/4 eculizumab (d). CIU fingerprints are depicted in the upper panels. ATDs extracted at 150 V corresponding to the three therapeutic mAbs are depicted in the lower panels (e, f, g, and h). Table summarizing the IM drift times of the observed unfolding states (i).

317x234mm (150 x 150 DPI)

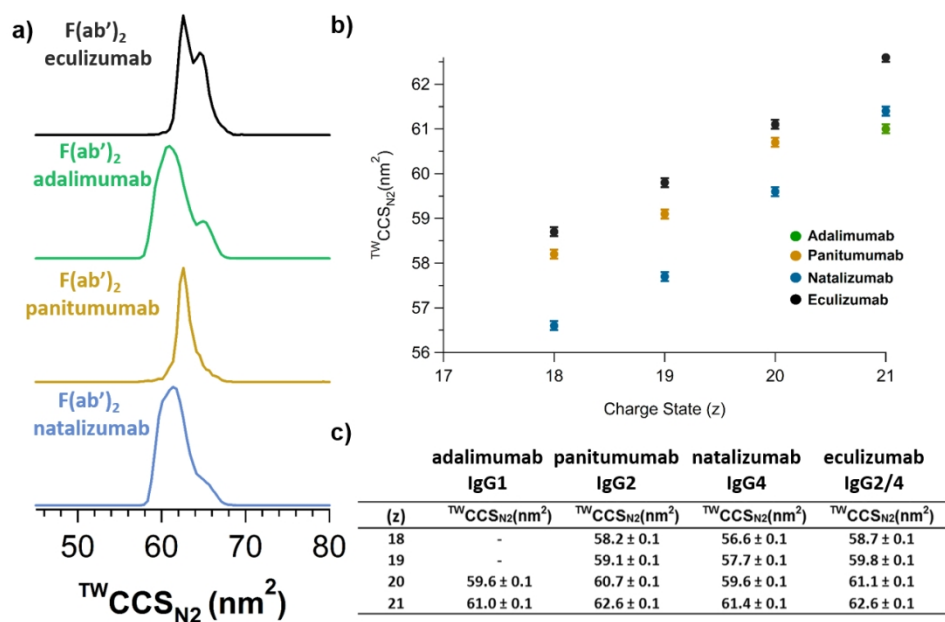


Figure 3: Middle-level IM-MS analysis of F(ab')₂ do-mains. CCSDs of the 21+ charge state of the F(ab')₂ domains of eculizumab, adalimumab, panitumumab, and natalizumab (a). Evolution of the F(ab')₂ TWCCSN₂ as a function of the charge state (b). Table summarizing the measured TWCCSN₂ of the F(ab')₂ domains (c).

231x148mm (150 x 150 DPI)

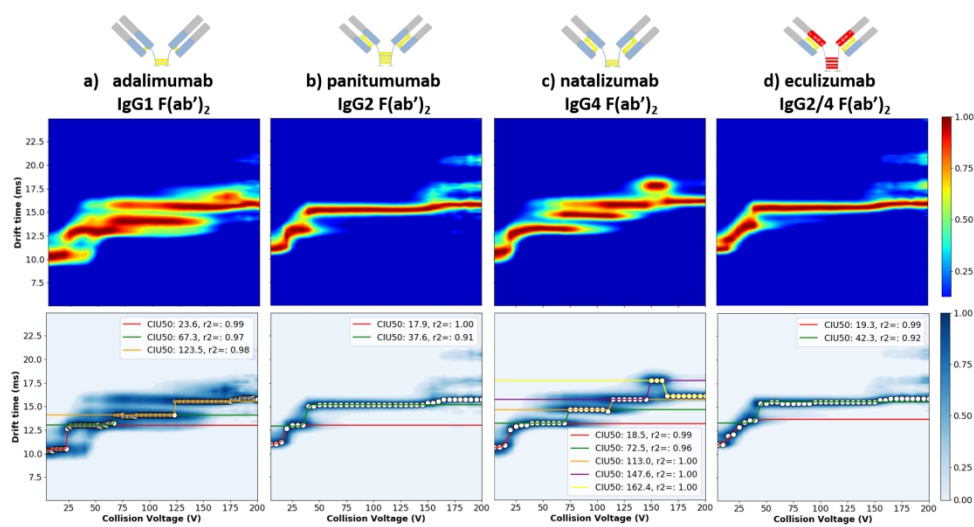
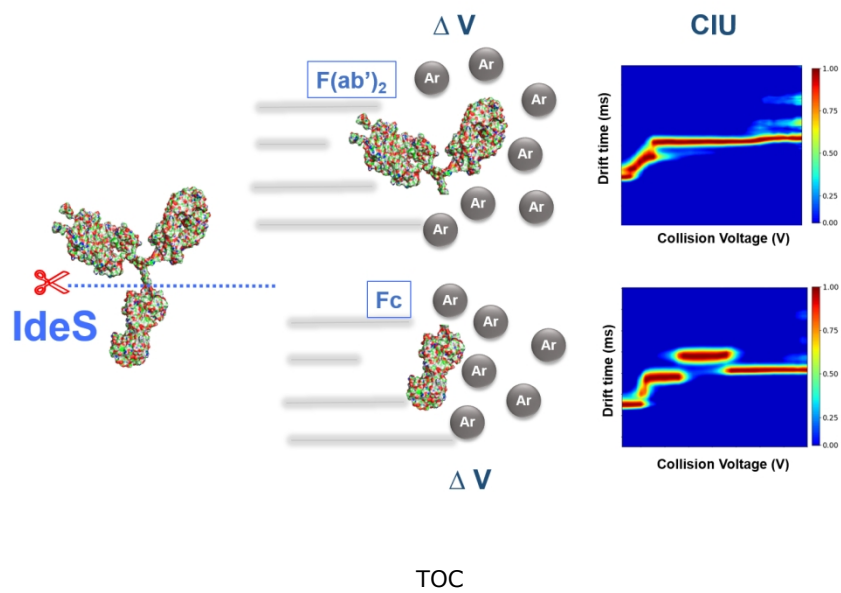


Figure 4: Middle-level CIU experiments on F(ab')₂ domains. CIU fingerprints (top panel) and stability analysis "CIU50" of 21+ charge state of F(ab')₂ domain of IgG1 (a), IgG2 (b), IgG4 (c), and IgG2/4 (d) from 0 to 200 V trap collision voltage. Gaussian fitting and collision voltages associated with the unfolding transitions are depicted in the lower panels

328x176mm (150 x 150 DPI)



TOC
309x176mm (150 x 150 DPI)